Guzmics, T., Berkesi, M., Bodnar, R.J., Fall, A., Bali, E., Milke, R., Vetlényi, E., and Szabó, C., 2019, Natrocarbonatites: A hidden product of three-phase immiscibility: Geology, https://doi.org/10.1130/G46125.1

SUPPLEMENTARY MATERIALS

1. DATA AND RESULTS

1.1. Sampling and Inclusion Petrography

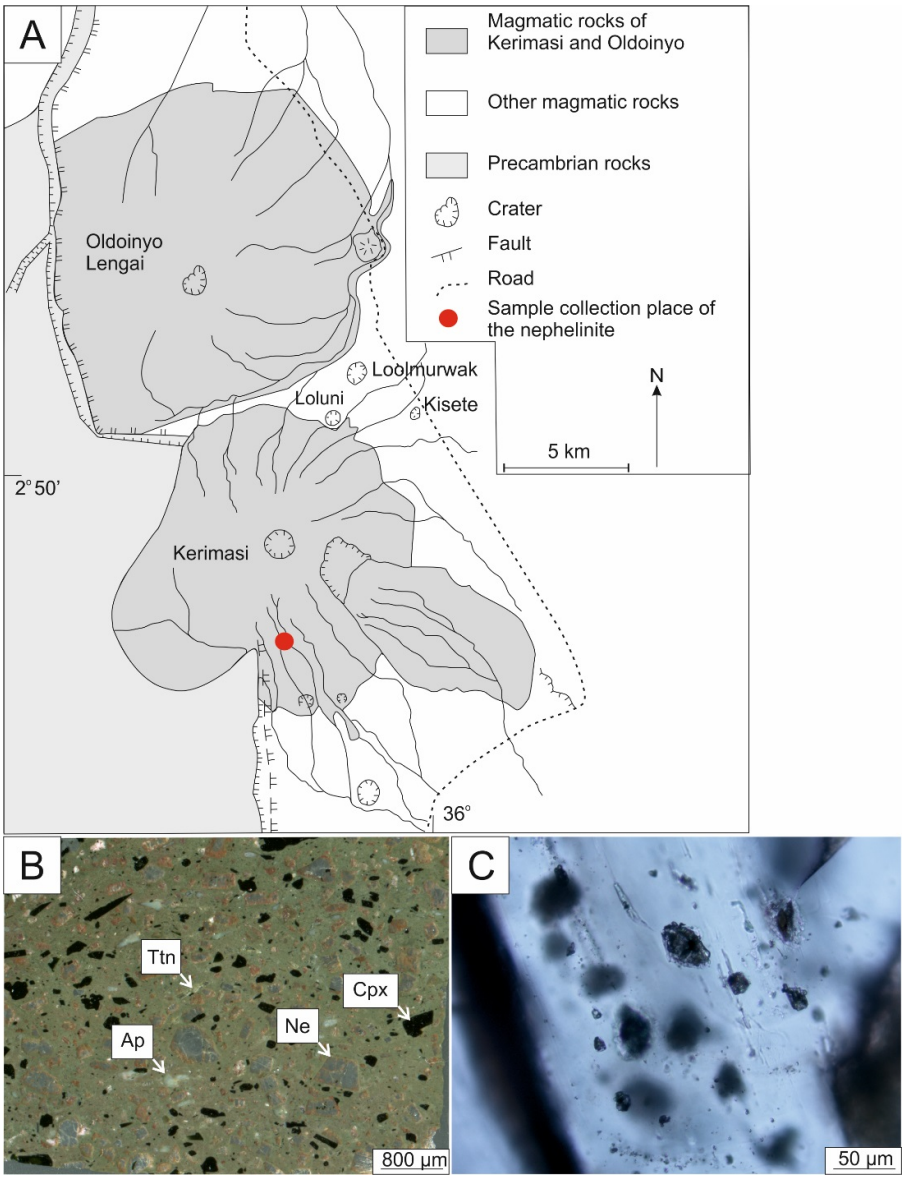

Fig. DR1. A: Schematic geological map of Kerimasi volcano and its environment (modified from Hay 1983). Red circle shows the location of the studied nephelinite body (2°54'20.4"S; 35°56'35.1"E, 1463m a.s.l.). **B:** Representative photomicrograph of the studied nephelinite of volcanic texture containing phenocrysts of Ap-apatite, Cpx-clinopyroxene (aegirine-augite), Ne-nepheline and Ttn-titanite**. C:** Representative photomicrograph (at room temperature) of the studied (unheated and undefined) melt and fluid inclusions that occur along growth zones of nepheline phenocrysts. The somewhat fuzzy and non-distinct features of the inclusions are the result of the well-crystallized nature of the inclusions. Determining the compositions of the entrapped melts and fluid phases in such inclusions is not possible, and they must be heated to homogenize the melt phases before analysis.

1.2. Microthermometry

During heating of fluid inclusions (Fig. DR2), the volume of the vapor phase increased at the expense of the solid phases in the temperature range 130 to ~178 ^{o}C. Carbonate liquid did not form during this heating event. Upon further heating, an alkali carbonate liquid phase formed at 340-365 ^{o}C, in coexistence with the vapor phase. The alkali carbonate liquid and vapor in the fluid inclusions homogenized to the liquid phase only in the smaller (2-3 μm) fluid inclusions, at a minimum temperature of 840 °C.

During heating of melt inclusions (Fig. DR3), a carbonate melt phase formed at 590-600 ^{o}C. With continued heating to 630-650 ^{o}C, the melt inclusions showed immiscible silicate-carbonate melts coexisting with a high proportion of solid phases and a fluid bubble. Two phases were observed in the fluid bubble, and the vapor was always surrounded by a liquid phase. Homogenization of the liquid and vapor to the liquid phase was recognized only in the smaller (1-2 μm) fluid bubbles at a minimum temperature of 840 °C. The last solid phase dissolved into the silicate melt at a maximum temperature of 838 °C, and the melt inclusions showed negative crystal shape. At 845-850 ^{o}C the fluid bubble homogenized into either the silicate or the carbonate melt only in melt inclusions that showed the lowest fluid bubble/melt volume ratios. At 850 ^{o}C only three phases were present in the majority of the nepheline-hosted melt inclusions, including a fluid-bubble, a silicate melt, and a carbonate melt, in highly variable volume fractions. All of these observations are evidence of heterogeneous entrapment of coexisting silicate melt, carbonate melt and a fluid. This interpretation suggests that melts and fluid entrapment occurred at a temperature above the dissolution temperature of the last solid phase at 838 ^{o}C, but close to the minimum temperature of dissolution of the fluid-bubble into the melts (845-850 ^{o}C). Accordingly,

entrapment of the melt(s) and fluid phase as inclusion in the nepheline likely occurred at ~850 °C.

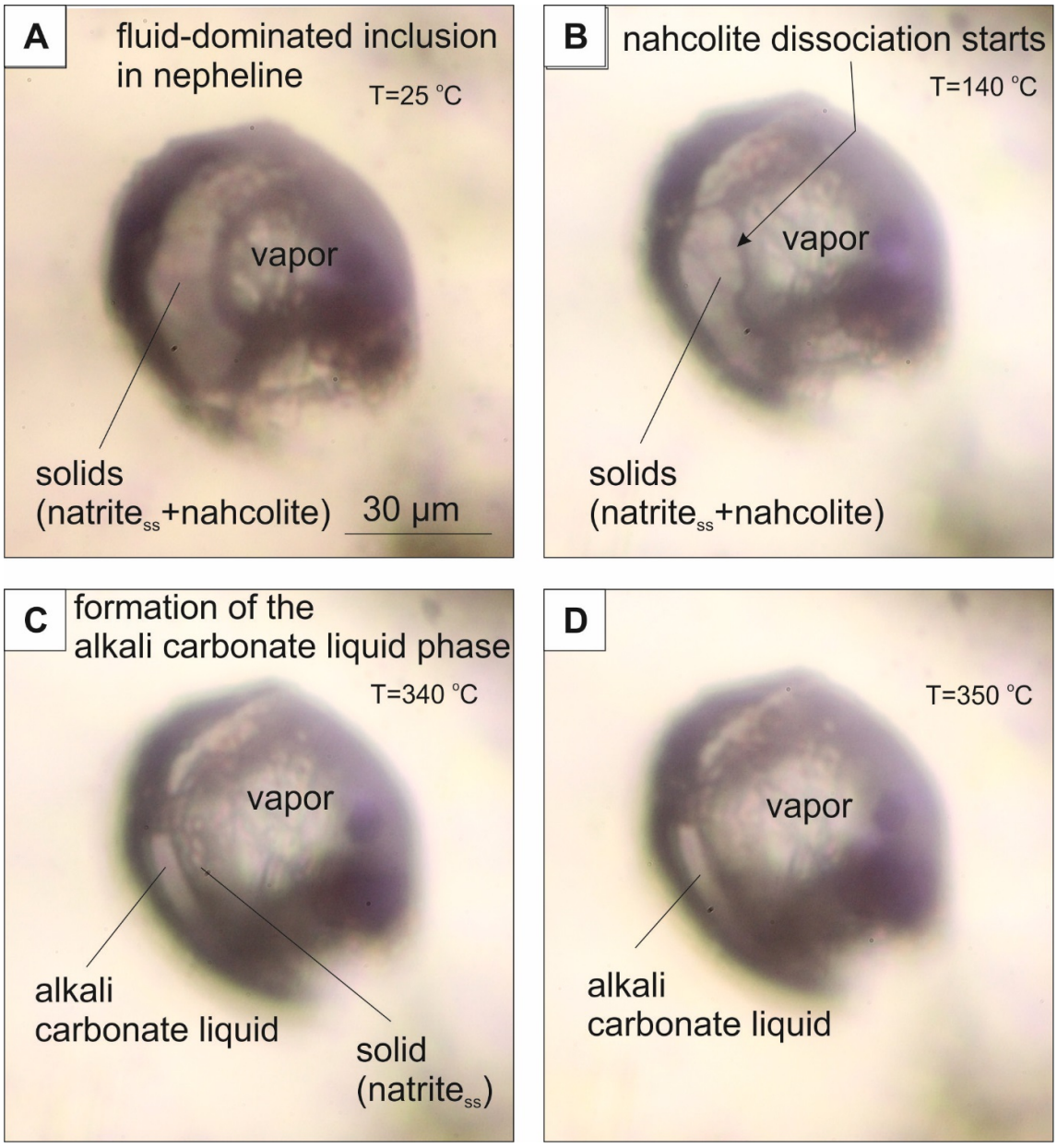

Fig. DR2. Representative photomicrographs taken during microthermometry on a nepheline-hosted, fluid-dominated inclusion, focusing on the visible phase transitions at low (< 400 °C) temperatures. **A:** The inclusion contains solid phases (predominantly natrite$_{ss}$ and nahcolite) and vapor CO_2 at 25 °C, as determined by Raman (see Fig. 3 and Fig. DR5-6). **B:** During heating, nahcolite dissociation started at 140 °C and terminated at 178 °C to produce natrite + CO_2 + H_2O. **C:** Alkali carbonate liquid starts to form at 340 °C by melting of natrite$_{ss}$. **D:** Continuation of melting of natrite$_{ss}$. natrite$_{ss}$ – natrite solid solution

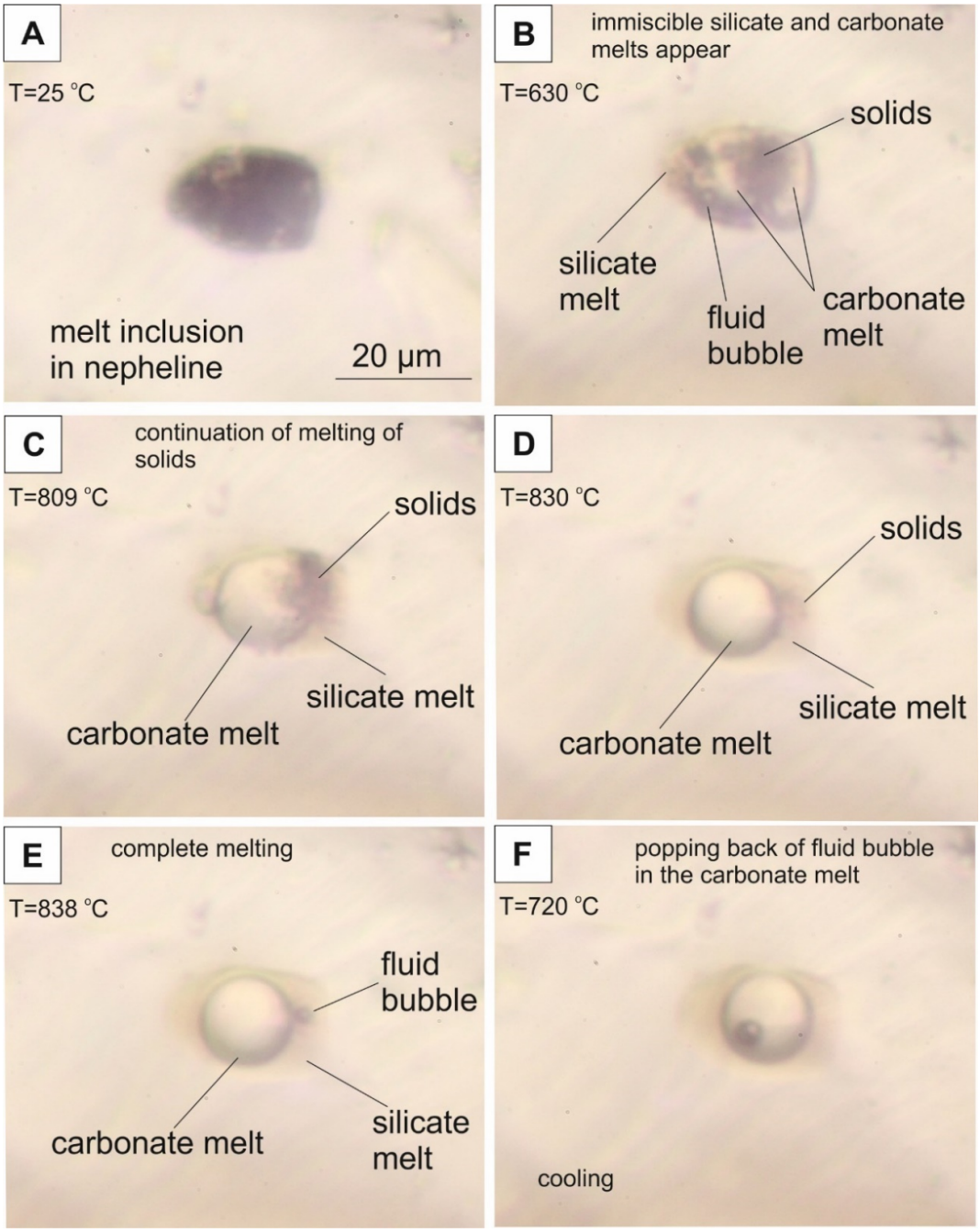

Fig. DR3. Representative photomicrographs taken during microthermometry on a nepheline-hosted melt inclusion. **A:** At room temperature the melt inclusion is fully crystallized. **B:** Immiscible silicate and carbonate melts appear at 630 °C. Before this observation, the final melting of solid carbonates was detected at 590 °C. **C-D:** Progressive melting of silicate phases in the silicate melt phase on further heating. Carbonate melt phase forms a full meniscus interface with the silicate melt. Note that the fluid bubble is still present but is hidden by the carbonate melt phase. **E:** Complete melting of the melt inclusion. Dissolution of the fluid bubble into the silicate melt phase at 845 °C. **F:** On cooling, the fluid bubble suddenly re-appears (rather than growing back slowly and continuously), suggesting complete dissolution of the fluid phase into both melt phases at 845 °C.

1.3. Run Products from Furnace Experiment

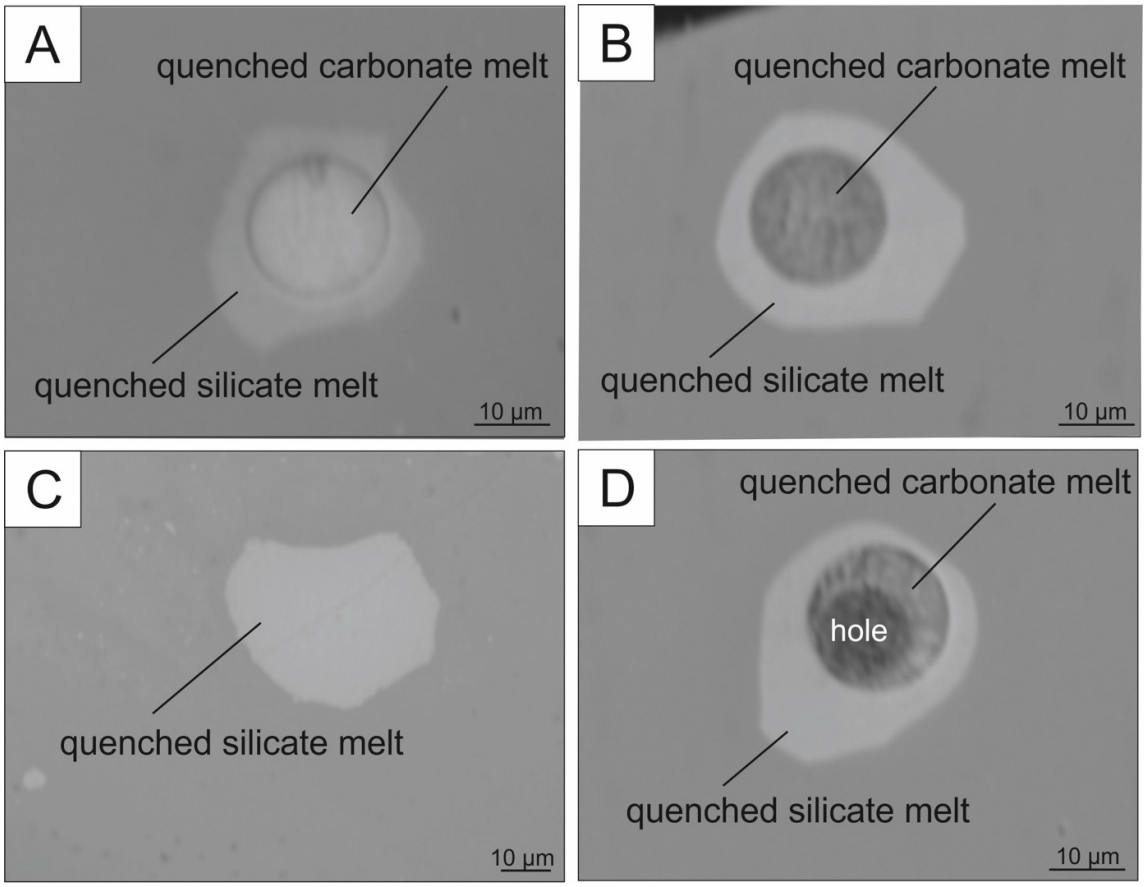

Fig. DR4. Representative back-scattered electron images on the quenched (850 ^{o}C) and exposed nepheline-hosted melt inclusions. **A, B:** Melt inclusions containing quenched immiscible silicate and carbonate melts. **C:** Melt inclusion containing quenched silicate melt. **D:** Melt inclusion containing quenched silicate and carbonate melts together with a former fluid bubble (hole) now filled by polishing powder. Fluid condensate was lost during polishing. The silicate melts quenched to a glass, the carbonate melts quenched to a microcrystalline assemblage.

1.3.1. Composition of the quenched carbonate and silicate melts determined by EMPA

Table DR1. Compositions of the quenched (850 °C) nepheline-hosted carbonate melts determined by EPMA (in wt%).

No.	1	2	3	4	5	6	7	8	9	10	11	12	13	14	15	16	17	18	*Average*	*1σ*
SiO_2	0.22	0.60	0.38	0.80	0.78	1.25	1.44	1.52	0.23	1.33	0.17	1.25	0.81	0.51	0.83	1.89	0.56	1.43	*0.89*	*0.51*
TiO_2	nd	0.11	0.04	0.03	0.03	0.37	0.09	nd	0.01	0.26	0.07	0.43	0.01	0.11	0.43	0.44	0.22	0.41	*0.17*	*0.17*
Al_2O_3	0.04	0.03	0.88	0.26	0.39	0.18	0.05	0.08	0.07	0.77	0.45	0.03	0.15	0.06	0.14	0.02	0.09	1.04	*0.32*	*0.38*
FeO^T	0.65	1.13	1.44	1.33	0.64	0.89	0.79	0.26	0.62	1.10	0.62	1.41	1.20	1.20	0.89	3.18	0.73	1.76	*1.10*	*0.64*
MnO	0.18	0.20	0.33	0.25	0.13	0.14	0.05	0.28	0.20	0.21	0.16	0.78	0.24	0.19	0.15	0.38	0.16	0.48	*0.25*	*0.17*
MgO	0.85	0.75	0.46	0.22	0.37	1.04	0.60	0.36	0.57	0.37	0.15	1.32	0.64	0.64	0.64	1.29	0.53	1.53	*0.68*	*0.39*
SrO	1.85	1.45	1.28	1.45	2.23	1.48	1.79	0.91	1.13	1.38	1.36	1.79	1.34	1.12	1.22	1.47	1.34	1.76	*1.46*	*0.32*
CaO	37.60	37.93	37.77	39.86	36.81	40.77	40.05	32.95	34.93	38.01	39.30	31.47	35.82	29.20	34.61	33.97	34.21	30.21	*35.86*	*3.42*
BaO	0.93	0.85	0.59	0.58	1.28	1.05	0.87	0.14	0.45	1.06	0.30	1.61	0.69	0.77	0.62	1.11	0.60	1.49	*0.83*	*0.39*
Na_2O	12.12	10.46	12.50	10.63	12.86	8.38	8.77	17.24	16.13	12.23	13.11	14.89	12.76	20.51	15.64	13.25	16.08	13.69	*13.40*	*3.02*
K_2O	3.55	3.99	1.13	2.87	3.32	2.91	2.78	4.46	3.46	2.08	1.86	1.78	3.41	3.41	3.10	1.87	3.47	4.27	*2.98*	*0.92*
P_2O_5	3.82	1.94	2.09	1.69	2.07	2.30	1.93	2.93	1.65	2.31	3.91	2.90	1.88	1.67	2.42	1.65	3.01	2.39	*2.36*	*0.70*
F	9.46	6.80	13.25	5.63	11.42	7.77	8.87	7.31	6.03	8.68	11.14	12.55	5.28	6.99	5.12	8.98	8.82	14.32	*8.80*	*2.78*
SO_3	1.98	3.08	4.65	1.47	3.27	1.79	3.20	2.33	1.98	1.78	3.97	3.63	2.44	4.05	3.31	1.60	3.19	4.91	*2.92*	*1.06*
Cl	0.68	1.95	1.24	0.55	1.79	1.21	1.70	0.17	0.93	4.23	0.67	0.70	1.69	2.56	1.88	1.29	2.61	1.49	*1.52*	*0.95*
Total	73.92	71.27	78.03	67.61	77.36	71.51	72.97	70.91	68.39	75.78	77.23	76.53	68.36	72.97	71.00	72.36	75.61	81.18	*73.55*	*3.67*
CO_2^*	26.08	28.73	21.97	32.39	22.64	28.49	27.03	29.09	31.61	24.22	22.77	23.47	31.65	27.03	29.01	27.64	24.39	18.82	*26.45*	*3.67*

FeO^T total Fe reported as FeO
Oxide values are corrected according to 2F=O and 2Cl=O
* CO_2 as carbonate represents difference to 100
nd not detected
1σ absolute standard deviation

Table DR2. Compositions of the quenched (850 °C) nepheline-hosted silicate melts determined by EPMA (in wt%).

No.	1	2	3	4	5	6	7	8	9	10	11	12	13	14	15	16	17	18	19	20	21	22
ǂ											6	7			11		12	14				
SiO_2	54.55	50.21	53.37	51.69	52.24	54.02	52.90	54.54	50.03	53.60	55.52	49.46	51.09	54.05	51.69	51.59	59.79	52.61	50.17	47.62	52.63	50.86
TiO_2	1.72	1.35	1.33	2.19	2.10	1.42	2.64	2.23	2.06	1.49	2.50	2.23	3.59	2.02	3.74	2.13	0.79	1.93	2.28	2.13	1.91	1.90
Al_2O_3	11.15	12.49	12.29	11.48	11.55	10.65	11.63	12.03	12.60	11.33	13.55	7.39	7.86	10.47	10.64	12.50	14.22	12.06	11.18	9.72	11.21	10.83
FeO^T	12.87	7.54	9.86	7.98	8.02	10.72	9.27	7.40	10.98	7.70	5.77	7.27	10.91	9.52	9.64	9.14	6.39	9.25	6.78	8.79	9.18	9.41
MnO	0.37	0.26	0.36	0.29	0.32	0.37	0.43	0.37	0.33	0.40	0.26	0.45	0.42	0.26	0.34	0.27	0.30	0.37	0.26	0.44	0.42	0.38
MgO	1.38	0.66	0.48	0.77	0.90	0.57	1.07	0.48	0.52	0.45	0.69	0.86	0.85	0.63	0.58	0.71	0.33	0.52	0.55	0.50	0.52	0.73
SrO	0.29	0.19	0.16	0.29	0.30	0.24	0.29	0.40	0.24	0.53	0.25	0.51	0.34	0.29	0.18	0.23	0.13	0.19	0.38	0.39	0.29	0.21
CaO	2.96	4.73	3.26	4.48	4.63	3.71	5.27	6.16	6.02	7.09	6.55	10.69	9.48	6.95	6.47	5.95	1.62	5.42	6.93	5.04	4.00	3.96
BaO	0.29	0.12	0.32	0.20	0.17	0.18	0.17	0.26	0.12	0.23	0.14	0.16	0.11	0.14	0.05	0.11	0.23	0.08	0.19	0.29	0.17	0.16
Na_2O	5.15	11.98	8.02	9.96	9.37	7.40	5.28	5.80	7.21	6.80	5.30	10.83	6.79	7.05	7.92	7.26	6.08	7.99	11.57	9.83	8.66	10.05
K_2O	6.19	6.98	6.49	6.15	6.06	6.43	6.21	5.84	5.66	6.60	6.04	4.37	4.35	4.96	4.40	6.34	7.42	5.42	5.28	6.79	6.62	6.65
P_2O_5	0.26	0.08	0.07	0.44	0.25	0.21	0.29	0.14	0.35	0.16	0.10	0.29	0.34	0.15	0.19	0.16	0.17	0.19	0.17	0.47	0.25	0.34
F	1.01	2.01	1.45	2.61	2.62	1.25	1.80	3.02	1.41	1.48	2.32	4.56	2.10	1.83	2.13	1.71	1.30	1.91	2.51	1.28	1.27	1.64
SO_3	0.16	0.34	0.79	0.55	0.58	1.01	1.12	0.62	0.78	0.71	0.17	0.76	0.45	0.40	0.85	0.42	0.06	0.82	0.95	3.07	1.12	1.19
Cl	0.05	0.36	0.65	0.45	0.41	0.61	0.82	0.39	0.53	0.51	0.33	0.64	0.40	0.37	0.43	0.47	0.26	0.40	0.44	2.81	0.75	0.82
Total	98.41	99.30	98.89	99.52	99.52	98.77	99.17	99.68	98.85	99.06	99.48	100.45	99.07	99.11	99.24	98.98	99.08	99.16	99.63	99.19	98.98	99.12

Table DR2 continued

No.	23	24	25	26	27	28	29	30	31	32	33	34	35	36	37	38	39	40	41	42	*Average*	*1SD*
ǂ							15			16			17		18							
SiO_2	56.68	52.65	53.16	49.68	49.09	50.13	51.18	57.40	54.49	51.58	55.29	53.93	48.58	49.55	56.96	53.86	51.02	52.54	52.19	48.53	*52.42*	*2.78*
TiO_2	1.45	1.95	1.01	3.22	3.38	3.38	3.05	1.80	2.01	2.21	0.75	1.67	4.29	3.00	1.65	1.64	0.98	2.15	2.03	1.44	*2.15*	*0.94*
Al_2O_3	13.52	12.84	12.04	13.49	13.58	13.88	11.66	13.69	11.45	12.26	15.96	15.45	8.74	11.04	13.21	13.06	12.57	11.05	12.28	12.28	*12.70*	*1.59*
FeO^T	5.34	8.53	9.11	7.94	7.84	7.80	9.50	7.22	8.58	9.37	5.88	7.41	10.05	9.53	6.15	8.39	7.68	8.48	8.02	9.71	*8.13*	*1.29*
MnO	0.28	0.29	0.28	0.34	0.25	0.23	0.33	0.41	0.43	0.30	0.26	0.39	0.41	0.33	0.33	0.38	0.29	0.29	0.26	0.29	*0.32*	*0.06*
MgO	0.21	0.66	0.56	0.45	0.48	0.43	0.60	0.41	0.43	0.48	0.35	0.41	0.82	0.66	0.48	0.47	0.43	0.67	0.65	0.72	*0.52*	*0.15*
SrO	0.26	0.13	0.23	0.16	0.15	0.22	0.28	0.10	0.10	0.19	0.06	0.06	0.45	0.27	0.11	0.16	0.31	0.29	0.23	0.21	*0.20*	*0.10*
CaO	3.30	2.35	2.64	5.50	5.53	5.62	6.64	1.80	2.24	5.58	1.33	1.57	9.59	6.08	2.16	2.21	4.80	3.60	3.52	3.28	*3.97*	*2.13*
BaO	0.14	0.10	0.18	0.10	0.10	0.03	0.26	0.10	0.17	0.13	0.26	0.14	0.23	0.06	0.15	0.09	0.31	0.20	0.18	0.12	*0.15*	*0.07*
Na_2O	9.64	9.82	10.24	8.92	9.29	8.21	7.32	6.63	10.59	9.48	10.25	9.16	7.35	9.85	8.72	10.19	9.85	10.20	10.01	11.62	*9.37*	*1.22*
K_2O	6.51	6.87	6.90	5.85	5.72	5.69	4.92	7.37	6.35	4.22	6.42	6.40	4.55	5.39	6.94	5.94	6.69	6.51	6.76	7.55	*6.18*	*0.89*
P_2O_5	0.02	0.12	*nd*	0.31	0.41	0.31	0.35	0.04	0.26	0.21	0.16	0.16	0.48	0.26	0.10	0.17	0.15	0.16	0.13	0.15	*0.21*	*0.12*
F	1.01	1.70	1.25	1.71	1.89	1.76	2.05	1.46	1.72	1.50	1.57	1.60	2.83	1.85	1.74	1.35	3.42	1.30	1.43	2.34	*1.77*	*0.56*
SO_3	0.59	0.59	0.71	0.99	1.04	0.97	0.60	0.34	0.08	0.98	0.32	0.29	0.63	0.71	0.24	0.64	0.90	0.94	0.85	0.51	*0.64*	*0.28*
Cl	0.39	0.55	0.59	0.42	0.40	0.42	0.42	0.31	0.19	0.49	0.45	0.47	0.47	0.52	0.27	0.51	0.49	0.64	0.58	0.42	*0.45*	*0.11*
Total	98.92	99.16	98.92	99.07	99.14	99.07	99.13	99.08	99.09	98.97	99.29	99.12	99.46	99.08	99.22	99.04	99.88	99.01	99.11	99.16	*99.15*	*0.21*

†$D^F_{CARB-SIL}$	Min.	1.9
	Max.	9.6

FeO^T total Fe reported as FeO
Oxide values are corrected according to 2F=O and 2Cl=O
nd not detected
1σ absolute standard deviation
ǂ No. of the coexisting carbonate melt in Table DR1
† Minimum-maximum values for the distribution coefficients of fluorine between the coexisting carbonate and silicate melts

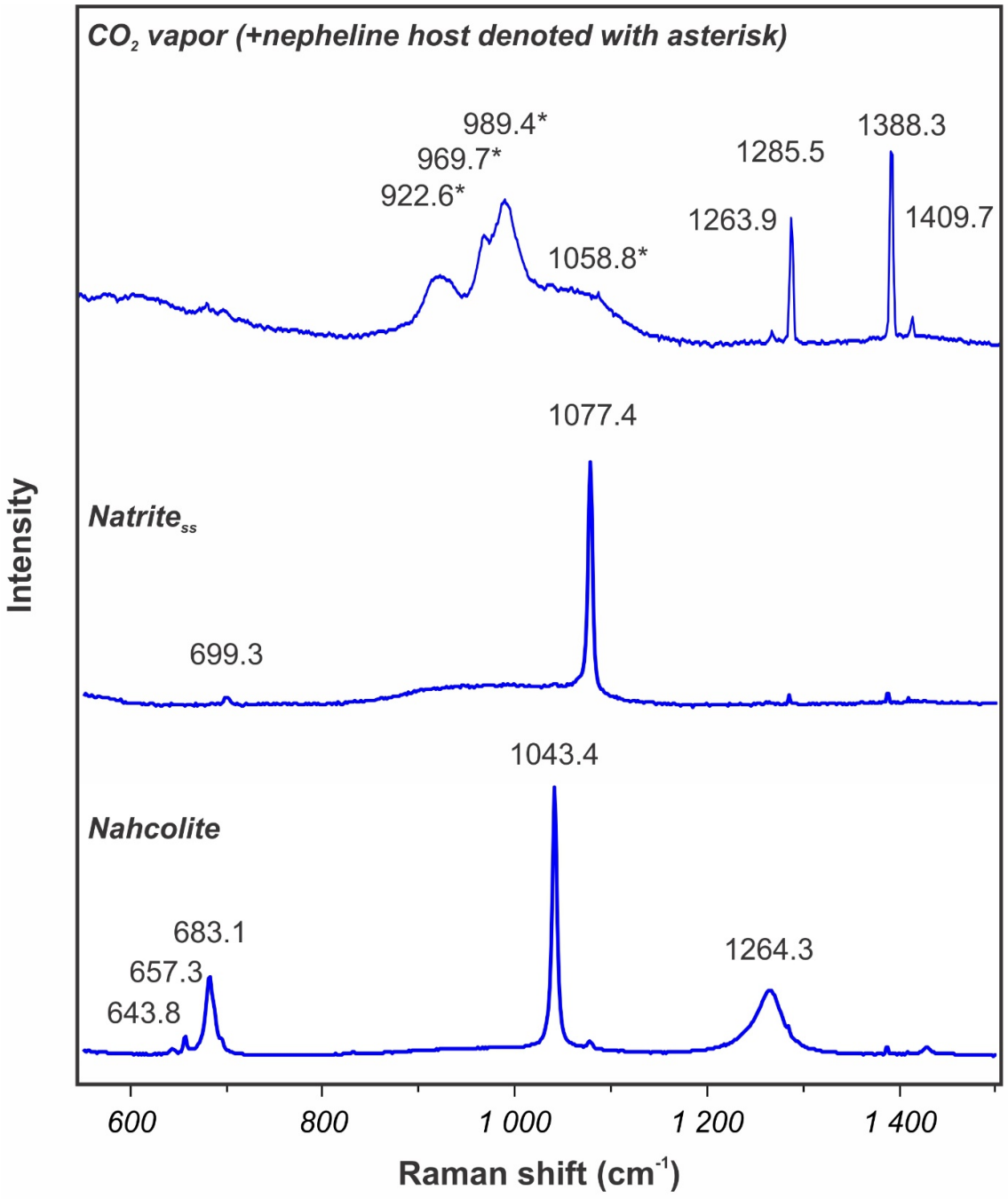

1.4. Results from Raman Spectroscopy on the Fluid Phases

Fig. DR5. Representative Raman spectra of the CO_2 vapor and fluid condensate (natrite$_{ss}$ + nahcolite) collected at room temperature from a fluid bubble in the quenched silicate melt phase in nepheline-hosted melt inclusion. Numbers indicate Raman band positions. Numbers with asterisk denote Raman bands of host nepheline. natrite$_{ss}$ – natrite solid solution

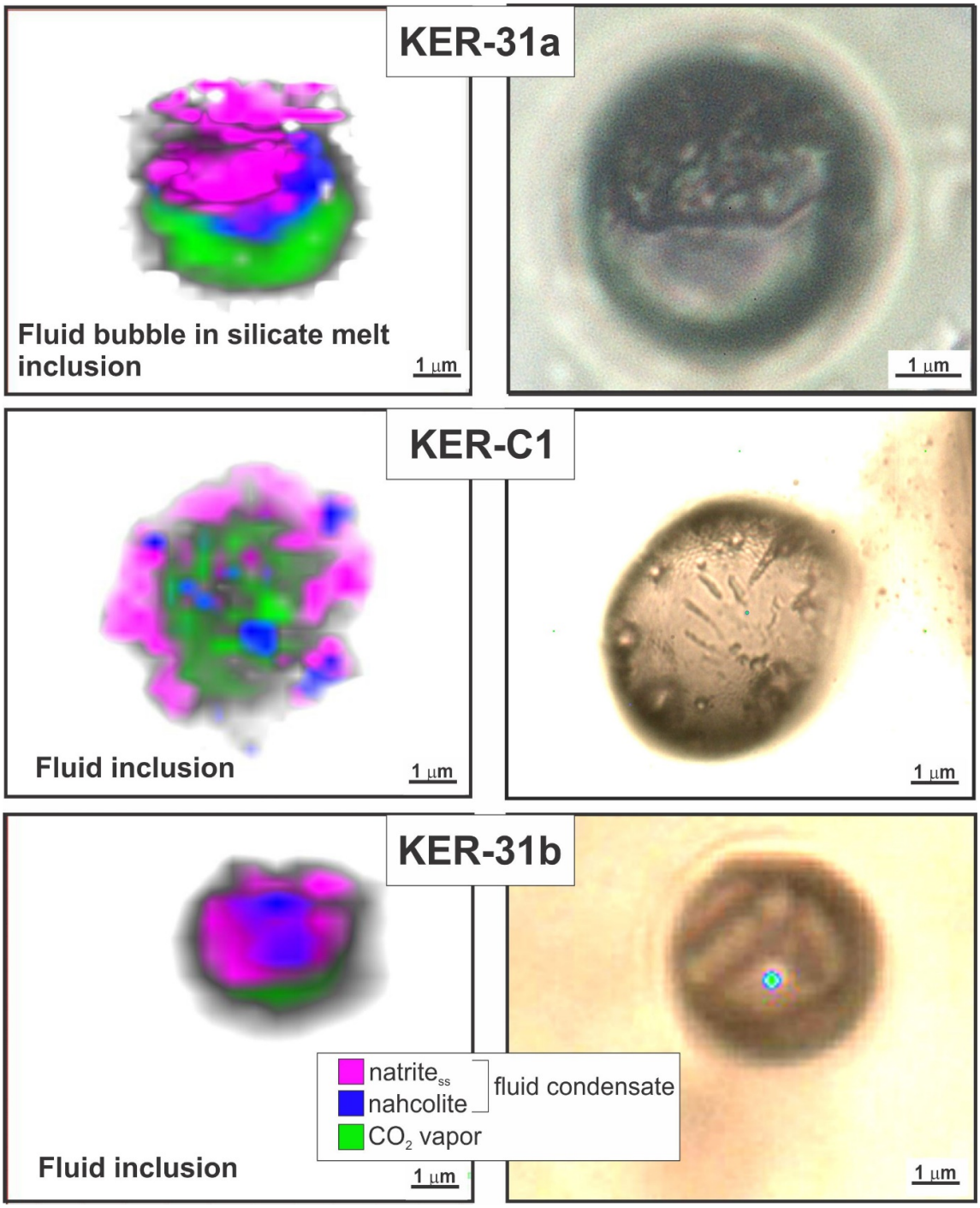

Fig. DR6. Representative X-Y Raman images (left column) and photomicrographs (right column) collected at room temperature on the nepheline-hosted fluid phases quenched from 850 ^{o}C. **KER-31a:** Fluid bubble in quenched silicate melt inclusion (shown in Figs. 1C and 2). **KER-C1 and KER-31b:** Fluid inclusions. All studied fluid bubbles in melt inclusions and fluid inclusions predominantly consist of natrite$_{ss}$ and nahcolite (called fluid condensate) and CO_2 vapor. natrite$_{ss}$ – natrite solid solution.

Table DR3. Raman data of nepheline-hosted fluid phases based on Raman images shown in Fig. DR6.

	fluid bubble in silicate melt inclusion				***fluid inclusion***				***fluid inclusion***			
Sample name	***KER-31a***				***KER-C1***				**KER-31b**			
Daughter phases (room temperature)	**nahcolite**	**natrite$_{ss}$**	**vapor CO_2**		**nahcolite**	**natrite$_{ss}$**	**vapor CO_2**		**nahcolite**	**natrite$_{ss}$**	**vapor CO_2**	
Number of pixels	***4557***	***6175***	***16496***		***21318***	***35914***	***23948***		***16571***	***25046***	***3710***	
Area%	***16.7***	***22.7***	***60.6***		***26.3***	***44.2***	***29.5***		***36.6***	***55.3***	***8.2***	
Density (g/cm^3)	*2.20*	*2.54*			*2.20*	*2.54*			*2.20*	*2.54*		
	Vapor CO_2 Raman data (room temperature)											
	v1	***v2***	***Δ Fermi***	***density***	***v1***	***v2***	***Δ Fermi***	***density***	***v1***	***v2***	***Δ Fermi***	***density***
	cm^{-1}			***g/cm^3***	***cm^{-1}***			***g/cm^3***	***cm^{-1}***			***g/cm^3***
	1285.5	***1388.3***	***102.8***	***0.06***	***1286.0***	***1388.9***	***102.9***	***0.09***	***1285.6***	***1388.5***	***102.9***	***0.09***
	calculated data											
Mass%	*37.55*	*58.74*	*3.71*		*33.43*	*65.03*	*1.54*		*36.31*	*63.36*	*0.33*	
H_2O from nahcolite dissociation (wt%)	*4.02*				*3.58*				*3.89*			
All vapor CO_2 (wt%) ǂ	*13.54*				*10.29*				*9.84*			
Natrite$_{ss}$ / nahcolite (area ratio, room temperature)	*1.36*				*1.68*				*1.51*			
Natrite$_{ss}$ / nahcolite (mass ratio, room temperature)	*1.56*				*1.95*				*1.75*			

ǂ CO_2 vapor at room temperature + CO_2 vapor from nahcolite dissociation

ν1 and ν2 defines the position of the lower and upper Raman bands of Fermi diad

Δ Fermi is the distance in band position between ν1 and ν2

CO_2 vapor density is calculated on the basis of Δ Fermi by using the equation developed by Fall et al., 2011.

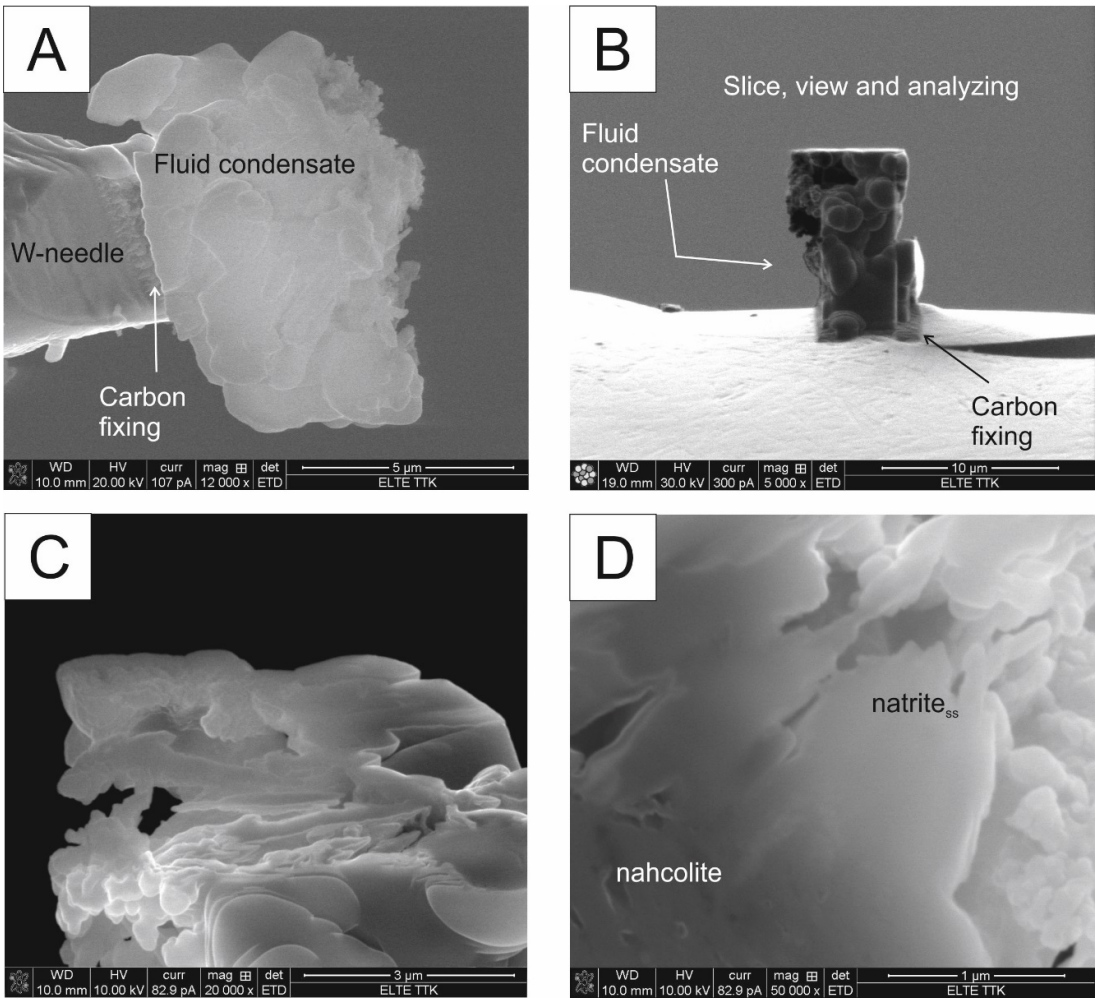

1.5. FIB-SEM-EDS Data on the Fluid Condensate in Sample KER-31a

Fig. DR7. Focused Ion Beam - Scanning Electron Microscopic study of the fluid condensate. These images show the fluid condensate (shown on Fig. 2B) after extraction from the fluid bubble using a nano-indentation method. **A**: Secondary electron image (SEI) of the fluid condensate attached to a W-needle by electron-vaporized carbon. **B**: Ion-beam image of the fluid condensate developed during the slicing process. **C**: High magnification view of the sliced surface (SEI). **D**: High magnification image to demonstrate the textural relationship between natrite$_{ss}$ and nahcolite (backscattered electron image). natrite$_{ss}$ − natrite solid solution.

Table DR4. Mass proportion of elements analyzed by EDS on the entire exposed surfaces of fluid condensate (Fig. DR7).

no. of slice	1	4	7	10	13	16	average	1σ
FeO^T	***1.0***	***0.7***	***0.6***	***1.0***	***0.9***	***1.1***	0.88	0.21
MgO	***0.6***	***0.3***	***0.6***	***0.9***	***0.9***	***1.7***	0.86	0.47
CaO	***8.8***	***4.0***	***12.9***	***13.1***	***14.2***	***16.5***	11.57	4.49
Na_2O	***73.8***	***78.4***	***72.2***	***67.3***	***68.2***	***62.9***	70.47	5.48
K_2O	***8.2***	***9.1***	***4.8***	***4.4***	***4.2***	***5.2***	5.99	2.10
BaO	***2.0***	***1.7***	***1.2***	***2.1***	***2.0***	***2.2***	1.87	0.39
P_2O_5	***0.2***	***-***	***0.5***	***0.8***	***2.2***	***-***	0.62	0.83
F	***2.5***	***3.7***	***5.1***	***5.6***	***5.8***	***7.3***	4.98	1.69
SO_3	***2.1***	***1.3***	***1.7***	***3.6***	***1.1***	***2.7***	2.10	0.93
Cl	***0.6***	***0.7***	***0.6***	***1.2***	***0.6***	***0.2***	0.65	0.32

FeO^T total Fe reported as FeO
One slice represents 250 nm, EDS data was collected after each 3 slicing steps (750 nm stepwise)
1σ absolute standard deviation

Table DR5. FIB-SEM volume data

Sample name	*KER-31a*		
Inclusion phase	(cavity=) vapor CO_2	fluid condensate = nahcolite + $natrite_{ss}$	halite
Volume%	***57.3-59.3***	***40-42***	***0.6-0.8***

2. CALCULATION

2.1. Compositional Range of the Fluid Phase in Sample KER-31a

Table DR6. Calculation of compositional range of the fluid phase (sample KER-31a). Eight variations of input parameters are shown providing the minimum and maximum values for the fluid components in wt%.

input parameters	Vapor CO_2 minimum Natrite/Nahcolite minimum Halite minimum Average - 1σ	Vapor CO_2 maximum Natrite/Nahcolite minimum Halite minimum Average - 1σ	Vapor CO_2 minimum Natrite/Nahcolite minimum Halite maximum Average + 1σ	Vapor CO_2 maximum Natrite/Nahcolite minimum Halite maximum Average + 1σ	Vapor CO_2 minimum Natrite/Nahcolite maximum Halite minimum Average - 1σ	Vapor CO_2 maximum Natrite/Nahcolite maximum Halite minimum Average - 1σ	Vapor CO_2 minimum Natrite/Nahcolite maximum Halite maximum Average + 1σ	Vapor CO_2 maximum Natrite/Nahcolite maximum Halite maximum Average + 1σ
phase name	input parameters in volume% (room temperature)							
$Natrite_{ss}$	24.2	23.1	24.1	22.9	26.4	25.2	26.3	25.1
Nahcolite	17.9	17.0	17.8	17.0	15.7	14.9	15.6	14.8
Halite	0.6	0.6	0.8	0.8	0.6	0.6	0.8	0.8
Vapor CO_2	57.3	59.3	57.3	59.3	57.3	59.3	57.3	59.3
Total	100.0	100.0	100.0	100.0	100.0	100.0	100.0	100.0
Fluid condensate = $natrite_{ss}$ + nahcolite	42.1	40.1	41.9	39.9	42.1	40.1	41.9	39.9
	calculated normative compositions in mass% (room temperature)							
$Natrite_{ss}$	58.21	58.05	57.91	57.74	63.13	62.96	62.84	62.67
Nahcolite	37.27	37.17	37.15	37.05	32.38	32.29	32.24	32.15
Halite	1.26	1.26	1.68	1.68	1.25	1.25	1.68	1.68
Vapor CO_2	3.26	3.53	3.26	3.53	3.23	3.50	3.23	3.50
Total	100.00	100.00	100.00	100.00	100.00	100.00	100.00	100.00
$Natrite_{ss}$/nahcolite (mass ratio)	1.56	1.56	1.56	1.56	1.95	1.95	1.95	1.95
	output data: calculated fluid components in wt%							
FeO^T	*0.42*	*0.41*	*0.51*	*0.50*	*0.42*	*0.42*	*0.52*	*0.52*
MgO								*0.63*

	0.24	*0.24*	*0.62*	*0.62*	*0.24*	*0.24*	*0.63*	
CaO	*4.38*	*4.37*	*7.48*	*7.46*	*4.47*	*4.46*	*7.64*	*7.62*
BaO	*0.92*	*0.91*	*1.05*	*1.05*	*0.94*	*0.93*	*1.08*	*1.07*
Na_2O	*40.84*	*40.73*	*35.87*	*35.77*	*41.73*	*41.61*	*36.64*	*36.54*
K_2O	*2.40*	*2.39*	*3.77*	*3.76*	*2.45*	*2.45*	*3.85*	*3.84*
P_2O_5	-	-	*0.68*	*0.68*	-	-	*0.69*	*0.69*
F	*2.04*	*2.03*	*3.11*	*3.10*	*2.08*	*2.08*	*3.17*	*3.17*
SO_3	*0.72*	*0.72*	*1.41*	*1.41*	*0.74*	*0.74*	*1.44*	*1.44*
Cl	*0.98*	*0.98*	*1.41*	*1.40*	*1.00*	*1.00*	*1.44*	*1.43*
CO_2	*43.14*	*43.30*	*40.22*	*40.39*	*42.51*	*42.67*	*39.54*	*39.70*
H_2O	*3.92*	*3.91*	*3.88*	*3.86*	*3.41*	*3.40*	*3.36*	*3.35*
Total	*100.00*	*100.00*	*100.00*	*100.00*	*100.00*	*100.00*	*100.00*	*100.00*
CO_2 as carbonate	*30.13*	*30.04*	*27.24*	*27.16*	*30.80*	*30.71*	*27.86*	*27.78*
Vapor CO_2 from nahcolite dissociation	*9.76*	*9.73*	*9.73*	*9.70*	*8.48*	*8.46*	*8.44*	*8.42*
All vapor CO_2 ǂ	*13.02*	*13.26*	*12.99*	*13.23*	*11.71*	*11.96*	*11.68*	*11.92*

FeO^T total Fe reported as FeO
Average (Table DR4)
1σ absolute standard deviation (Table DR4)
ǂ CO_2 vapor at room temperature + CO_2 vapor from nahcolite dissociation
$Natrite_{ss}$ natrite solid solution

Table DR7. Compositional range of the fluid phase (sample KER-31a, wt%). Minimum and maximum values are from Table DR6.

	minimum	maximum
FeO^T	*0.41*	*0.52*
MgO	*0.24*	*0.63*
CaO	*4.37*	*7.64*
BaO	*0.91*	*1.08*
Na_2O	*35.77*	*41.73*
K_2O	*2.39*	*3.85*
P_2O_5	-	*0.69*
F	*2.03*	*3.17*
SO_3	*0.72*	*1.44*
Cl	*0.98*	*1.44*
CO_2	*39.54*	*43.30*
H_2O	*3.35*	*3.92*
CO_2 as carbonate	*27.16*	*30.80*
Vapor CO_2 from nahcolite dissociation	8.42	9.76
All vapor CO_2 ǂ	11.68	13.26

FeO^T total Fe reported as FeO

ǂ CO_2 vapor at room temperature + CO_2 vapor from nahcolite dissociation

2.2. Average Composition of the Fluid Phase (Sample KER-31a)

Table DR8. Calculation of average composition of the fluid phase (sample KER-31a).

Phase name	input parameters in volume% (room temperature)
$Natrite_{ss}$	23.6
Nahcolite	17.4
Halite	0.7
Vapor CO_2	58.3
Total	100.0
Fluid condensate = $natrite_{ss}$ + nahcolite	41
	calculated normative composition in mass% (room temperature)
$Natrite_{ss}$	57.97
Nahcolite	37.17
Halite	1.50
Vapor CO_2	3.39
Total	100.00
$Natrite_{ss}$/nahcolite (mass ratio)	1.56
	output data: calculated fluid components in wt%
FeO^T	*0.47*
MgO	*0.45*
CaO	*6.14*
BaO	*0.99*
Na_2O	*37.95*
K_2O	*3.18*
P_2O_5	*0.33*
F	*2.64*

SO_3	*1.11*
Cl	*1.22*
CO_2	*41.62*
H_2O	*3.89*
Total	*100.00*
CO_2 as carbonate	*28.49*
Vapor CO_2 from nahcolite dissociation	*9.73*
All vapor CO_2 ǂ	*13.12*

FeO^T total Fe reported as FeO

ǂ CO_2 vapor at room temperature + CO_2 vapor from nahcolite dissociation

$Natrite_{ss}$ natrite solid solution

3. METHODS

3.1. Microthermometry and Furnace-heating Techniques

Nepheline-hosted melt inclusions are well crystallized, prohibiting phase identification by optical microscopy and limits compositional determination by electron microprobe (Fig. DR1 and DR3A). To remedy this problem, the fluid and melt phases in nepheline-hosted melt inclusions were heated and monitored during heating using a Linkam TS 1500 high-temperature stage mounted on a Nikon Eclipse E600 polarization microscope at the Lithosphere Fluid Research Laboratory, Eötvös University Budapest (Hungary). Microthermometric experiments were conducted on 45 inclusions in 7 nepheline grains. The heating rate was 10°C/min, with a maximum temperature of 1000°C. Uncertainty of reported temperatures does not exceed 2 degree Celsius.

We also carried out heating–quenching experiments on the melt inclusions using a Carl-Zeiss Jena high-temperature (1 atm) furnace to reproduce the characteristic melt and fluid phases that were present at the trapping time. Handpicked single nepheline grains were encapsulated in graphite containers to prevent oxidation during the experiments. Temperature during the experiments was 850°C, with an uncertainty of ±20 degrees Celsius, and the heating rate from room temperature was 15-20 degrees Celsius/min; in the melt inclusions quenched melts were produced with a quenching rate of 300–350°C/s. The quenched melt inclusions were exposed at the surface by polishing using dry corundum powder (Fig. DR4). After exposure the grains were placed in oil to prevent alteration of the quenched carbonate melts when in contact humid air.

3.2. Electron Microprobe Analyses

Major element compositions of the quenched melt phases within the melt inclusions were determined using a JEOL JXA 8200 Superprobe with five wavelength dispersive

spectrometers at the Free University, Berlin (Germany) (Table DR1-3). Oil was removed from the grains immediately before the analyses without using water. Quenched silicate and carbonate melts were analyzed with a 10 μm diameter beam. To minimize errors in sodium analyses associated with migration under exposure to the electron beam, this element was measured in the first 5 s of the analysis. The accelerating voltage and beam current were 15 kV and 20 nA, respectively. We collected data from 18 carbonate melts and 42 silicate melts from nepheline-hosted melt inclusions (Table DR1-3). Fluid condensate was lost during polishing, precluding its analyses by EMPA. Owing to the high concentrations of halogens in carbonate and silicate melts, we corrected the oxide wt% values according to 2(F+Cl) = O. The CO_2 content of the carbonate melts was calculated by difference from 100% totals. Natural standards were used for instrument calibration, and ZAF corrections were applied.

3.3. Raman Spectroscopy

Raman spectroscopic analyses were conducted mainly to determine fluid components in unexposed, nepheline-hosted inclusions at the Faculty of Science Research and Instrument Core Facility of Eötvös University, Budapest (ELTE FS-RICF), Hungary. We used a confocal HORIBA Labram HR (high resolution) 800 spectrometer with Nd:YAG laser (λ = 532 nm) excitation, 600 and 1800 gr/mm optical gratings, a 50–200 μm confocal hole, a 2–30 sec acquisition time, and a 100× objective. The laser spot size (lateral) was ~1.2 μm and the depth resolution was 1.7 μm, using a 50 μm confocal hole and 100× objective. The laser power was ~50 mW at the sample surface. The spectral resolution was 0.7 cm^{-1} and 3.6 cm^{-1} at 1398.5 cm^{-1} (full width at half maximum of one neon line) with the 1800 and 600 gr/mm gratings, respectively. Data manipulation (background fitting and peak fitting using the Gaussian–Lorentzian sum profiles) was carried out using LabSpec v5.5 software. For mineral and fluid identification, various published databases (Frezzotti et al, 2012, Golovin et al., 2017) were used.

Three different applications of Raman spectroscopy were used in this study, including:

1) Spot analyses of quenched melt inclusions at room temperature was conducted in the range that is characteristic of quenched silicate melt (between 850 and 1060 cm^{-1} and 3300-3700 cm^{-1}), quenched carbonate melt (v1-CO_3^{2-} band at around 1072 cm^{-1}, the main bands of dissolved SO_4^{2-} and PO_4^{3-} at around 994-998 cm^{-1} and 952 cm^{-1}, respectively) and fluid phase (CO_2 Fermi diad at 1285 and 1388 cm^{-1}, nahcolite at 1043-1046 and 1264-1265 cm^{-1} and natrite at 1077-1078 cm^{-1}) (Fig. DR5). Dissolved H_2O and CO_3^{2-} concentration in the quenched silicate melt were calculated using the method described by Zajacz et al. (2005) and Morizet et al. (2013), respectively. We calculated vapor CO_2 density (0.06-0.09 g/cm^3), based on the splitting of the Fermi diad using the calibration after Fall et al., 2011. To help with phase identifications, we collected control spectra from the host nepheline in the proximity of and from the same depth as the phases of interest in order to remove these interfering bands from the inclusion spectra.

2) Raman X-Y imaging of representative quenched fluid inclusions (n=2) and a silicate melt-hosted fluid bubble (n=1) was carried out with 0.5 μm stepwise focusing on the solid-rich portion of the bubble in the spectral range between 100 and 1760 cm^{-1} (Fig. DR6). A neon spectrum was collected before and after the imaging process to better calibrate the band positions. The minimum-maximum natrite/nahcolite area ratios (1.4-1.7) and CO_2 area percentages (8.2-60.6) were calculated based on the pixel number of the respective phase on the images using COREL PHOTO-PAINT 2017.

Daughter phase proportions of the fluid phases at room temperature estimated based on Raman images (n=3), considering the area percentages and the density of the phases (Table DR3), indicated 33.4-37.6% nahcolite, 58.8-65.0% natrite and 0.3-3.7% vapor CO_2, all in wt%. We also estimated that non-carbonate CO_2 represents 9.8-13.5 wt% (e.g. vapor CO_2

at room temperature + vapor CO_2 from nahcolite dissociation) and H_2O of 3.6-4.0 wt% (from nahcolite dissociation) in the fluid phase (Table DR3).

3) Raman spectroscopic analysis was also conducted during heating to 600°C in a Linkam THMS600 heating-cooling stage (Fig. 3) to confirm the low temperature phase transitions observed in the fluid inclusions. The accuracy of temperature determination was ±0.2 degrees Celsius. Raman spectra were collected at 21 °C, 100 °C, 200 °C, 400 °C and 600 °C (Fig. 3).

3.4. Focused Ion Beam – Scanning Electron Microscopy (FIB-SEM)

Focused ion beam–scanning electron microscopy (FIB–SEM) analysis was conducted at ELTE FS-RICF using an FEI QUANTA 3D FIB–SEM apparatus equipped with both secondary (SE) and backscattered electron (BSE) detectors, combined with an Apollo XP silicon drift energy dispersive spectrometer (EDS). The accelerating voltage and current used for the ion beam imaging was 30 kV and 50 pA, respectively, and a 5nA current was used during slicing. For electron beam analysis we used 15 kV and 50 pA-4 nA, which permitted analysis of major elements with masses ranging from beryllium through oxygen to barium.

A fluid bubble in a reheated and quenched melt inclusion (sample KER-31a shown in Fig. 1C and 2B), previous analyzed by Raman imaging (Fig. 2A) had a diameter of 13 μm and was located at a depth below the surface of less than 5 μm. The fluid condensate was successfully extracted after exposing the fluid bubble (Fig. 2B) by nano-indentation and using a W-needle and electron-vaporized carbon as glue (Fig. DR7A). After the solids in the fluid condensate had been attached to the W-nanoneedle, the fluid condensate was extracted from the fluid bubble and placed on carbon tape (Fig. DR7B). In this position, the fluid condensate was sliced in 250 nm increments. After each slicing step, the surface was examined by SEM (Fig. DR7C). We collected EDS spectra from the entire exposed surfaces after each 3 slicing

steps (750 nm stepwise, n=6, Table DR4). Based on the collected EDS spectra, we calculated the average mass proportion of major elements using the EDAX ZAF standardless quantification algorithm of the Genesis program package (Table DR4). Oxygen and carbon concentrations were not quantified.

3.5. Fluid phase Composition Calculation

The compositional range for the fluid phase (Table DR6-7) was estimated based on combined FIB-SEM-EDS analysis and Raman images of the same fluid bubble (sample KER-31a, shown in Figs. 1C, 2A-B, DR6). Results indicate 58.1-63.1 wt% $natrite_{ss}$, 32.2-37.3 wt% nahcolite, 1.2-1.7 wt% halite and 3.2-3.5 wt% CO_2 vapor (Table DR6). As input parameters for the calculation we used 1) the minimum-maximum range for $natrite_{ss}$/nahcolite area ratios (1.36-1.68, Table DR3) from the Raman images (n=3, Fig. DR6), 2) the fluid condensate-halite-CO_2 volume% (40-42, 0.6-0.8, 57.3-59.3, Table DR5) from FIB-SEM analyses of sample KER-31a and 3) the density (g/cm^3) of CO_2-vapor (0.06, Table DR3), nahcolite (2.20), natrite (2.54) and halite (2.17). As natrite and nahcolite phases cannot be clearly distinguished from one another by SE and BE images (Fig. DR7D), $natrite_{ss}$/nahcolite volume ratio was not determined during FIB-SEM slicing analysis. Taking into account the average mass proportion (± 1σ errors) of EDS-detected elements in fluid condensate (Table DR4) and the range in mass% of halite (1.25-1.68, Table DR6), we formed normative nahcolite, $natrite_{ss}$ and halite as required by their mass% ranges, using CO_2 and H_2O (Table DR6). Normative nahcolite was formed based on the reaction $Na_2O+H_2O+2CO_2 = 2NaHCO_3$. The excess Na and all other EDS-detected elements are used to form halite and $natrite_{ss}$ by charge balance. It was assumed that Cl^- and SO_4^{2-} react with Na^+, and that F^- and PO_4^{3-} with Ca^{2+}; the rest of Na^+ and Ca^{2+} and all additional cations (K^+, Ba^{2+}, Mg^{2+} and Fe^{2+}) form carbonates.

We also calculated the average fluid composition (Table DR8) by applying the same calculation method. As input parameters, we used the average mass proportion of EDS-detected elements in fluid condensate (Table DR4) and values for natrite$_{ss}$/nahcolite area ratio measured by Raman (1.36, Table DR3), and fluid condensate-halite-CO_2 volume% (41-0.7-58.3) mean values from FIB-SEM (Table DR6).

4. SUPPLEMENTARY MATERIAL REFERENCES

Fall, A., Tattitch, B., and Bodnar, R.J., 2011, Combined microthermometric and Raman spectroscopic technique to determine the salinity of H_2O–CO_2–NaCl fluid inclusions based on clathrate melting: Geochimica et Cosmochimica Acta, v. 75, p. 951-964.

Frezzotti, M-L., Tecce, F., and Casagli, A., 2012, Raman spectroscopy for fluid inclusion analysis: Journal of Geochemical Exploration, v. 112, p. 1–20.

Golovin, A. V., Korsakov, A.V., Gavryushkin, P.N., Zaitsev, A.N., Thomas, V.G., and Moine, B.N., 2017, Raman spectra of nyerereite, gregoryite, and synthetic pure $Na_2Ca(CO_3)_2$: diversity and application for the study micro inclusions: Journal of Raman Spectroscopy, v. 48, p. 1559-1565.

Morizet, Y., Brooker, R.A., Iacono-Marziano, G., and Kjarsgaard, B. A., 2013, Quantification of dissolved CO_2 in silicate glasses using micro-Raman spectroscopy: American Mineralogist, v. 98, p. 1788–1802.

Zajacz, Z., Halter, W., Malfait, W.M., Bachmann, O., Bodnar, R.J., Hirschmann, M. M., Mandeville, C.W., Morizet, Y., Müntener, O., Ulmer, P, Webster, J.D., 2005, A composition-independent quantitative determination of the water content in silicate glasses and silicate melt inclusions by confocal Raman spectroscopy: Contribution to Mineralogy and Petrology, v. 150, p. 631–642.